Acta Cryst. (1988). A**44**, 828-833

Triple-Crystal Diffraction Studies on Ion-Implanted and Other Silicon Crystals Using a Synchrotron Source

BY A. W. STEVENSON AND S. W. WILKINS

CSIRO, Division of Materials Science and Technology, Locked Bag 33, *Clayton, Victoria* 3168, *Australia*

J. HARADA

Department of Applied Physics, Nagoya University, Chikusa-ku, Nagoya 464, *Japan*

N. KASHIWAGURA

Department of Basic Sciences, Faculty of Engineering, Gifu University, Yanagido, Gifu 501-11, *Japan*

K. OHSHIMA

Institute of Applied Physics, University of Tsukuba, Sakura, Ibaraki 305, *Japan*

AND M. SAKATA

Department of Applied Physics, Nagoya University, Chikusa-ku, Nagoya 464, *Japan*

(*Received* 30 *November* 1987; *accepted* 18 *April* 1988)

Abstract

Triple-crystal diffraction studies are capable of cleanly separating the various experimental components of the scattering in the vicinity of a Bragg peak. The two-dimensional intensity distributions obtained in such an experiment consist of various components which extend in distinct directions in $(\Delta\omega_S, \Delta 2\theta_S)$ space, where $\Delta\omega_S$ and $\Delta 2\theta_S$ are the offset angles of the sample and analyzer/detector from the Bragg condition. One-dimensional 'slice' scans can be used in studying specific details, given a known disposition of the components, be they dynamical, kinematical or aspects of the instrumental arrangement. In this paper triple-crystal diffraction results obtained for given ion-implanted and other Si crystals using both a conventional X-ray tube and a synchrotron source are presented and compared.

Introduction

Triple-crystal X-ray diffractometry represents a high-resolution technique for investigating the detailed distribution of intensity in the vicinity of Bragg reflection peaks. Fig. 1 shows the sort of experimental arrangement which might be used for such a study and is in fact the one which was used for the synchrotron measurements reported in the present study. The 'first crystal' in this case is actually a double-crystal Si(111) monochromator, and the Si(111) sample and analyzer are such that the overall configuration is $(+n, -n, +n, -n)$. The two-dimensional intensity distribution about the Si 111 Bragg peak would be collected as a function of $\Delta\omega_S$ (the deviation of the sample rotation from the exact Bragg condition) and $\Delta\omega_A$ (for the analyzer crystal) or $\Delta 2\theta_S$ (the deviation of the receiving angle of the analyzer/detector combination about the sample from the exact Bragg condition).

Fig. 2(*a*) shows, in reciprocal space, the disposition of the axes for $\Delta\omega_S$ and $\Delta 2\theta_S$, and various other components of the scattering distribution. An examination of the theory for dynamical diffraction from a perfect crystal shows that the tail of the dynamical diffraction peak extends parallel to the crystal-surface normal as a result of the boundary condition on the tangential continuity of the fields at the beam exit surface. In the case of symmetrical Bragg reflection, this tail is also parallel to the scattering vector. The sample mosaic spread, a kinematical component, extends along a direction normal to the scattering vector in the plane of diffraction, while isotropic thermal diffuse scattering leads to a broad peak centred on the line $\Delta\omega_S = \Delta 2\theta_S/(2\sin^2\theta_B)$

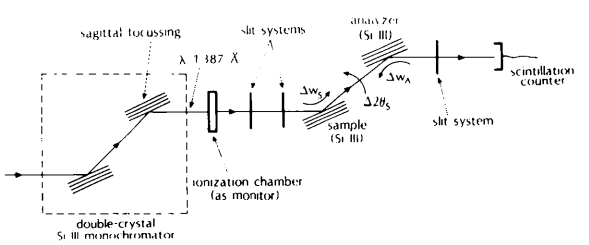

Fig. 1. Schematic diagram of the experimental arrangement used for the synchrotron measurements.

0108-7673/88/060828-06$03.00

($\Delta\omega_S = \Delta 2\theta_S/2$) for a $\Delta 2\theta_S$ ($\Delta\omega_S$) scan (*e.g.* Wilkins, Chadderton & Smith, 1983). Fig. 2(*a*) also displays the loci associated with the dynamical tail of the monochromator being Bragg reflected by the sample, and the dynamical tail of the analyzer and wavelength spread.

Fig. 2(*b*) shows the same information as in Fig. 2(*a*), but in angular space, where the $\Delta\omega_S$ and $\Delta 2\theta_S$ axes are orthogonal. The dynamical tails associated with monochromator, sample and analyzer are shown along the lines corresponding to $\Delta\omega_S = \Delta 2\theta_S$, $\Delta 2\theta_S/2$ and 0 respectively. Fig. 2(*b*) also shows the effect of surface roughness on the sample, where a (linear) variation in the FWHM of the Bragg tail is expected (Iida & Kohra, 1979). Thus, in addition to cleanly separating various components (normally convoluted together in, say, a double-crystal rocking curve), triple-crystal diffraction is an extremely sensitive probe of sample properties, especially in the near-surface region. Iida & Kohra (1979) also pointed out that other aspects of crystal imperfection such as lattice-parameter variation (along the direction $\Delta\omega_S = \Delta 2\theta_S/2$) and surface misorientation (along the $\Delta\omega_S$ direction) could be distinguished from surface roughness.

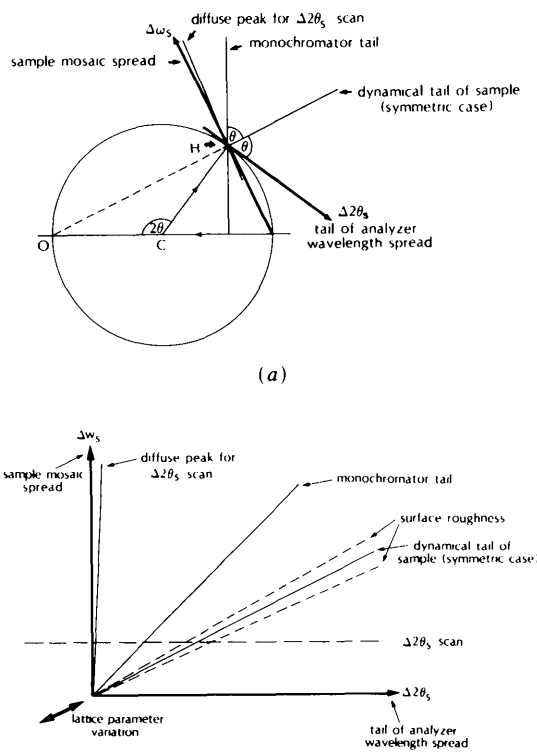

Fig. 2. Disposition of the $\Delta\omega_S$ and $\Delta 2\theta_S$ axes, and various other components of the scattering distribution for (*a*) reciprocal and (*b*) angular space. A $\Delta 2\theta_S$ 'slice' scan corresponds to a line parallel to that axis, a $\Delta\omega_S$ 'slice' scan being parallel to the $\Delta\omega_S$ axis.

The separation of dynamical and kinematical components of the scattering for nearly perfect crystals by introducing a perfect-crystal analyzer was demonstrated by Eisenberger, Alexandropoulos & Platzman (1972) and, later, by Iida & Kohra (1979). Simple theoretical treatments (*e.g.* Afanas'ev, Koval'chuk, Kovev & Kohn, 1977) show that the strain distribution in the near-surface region of a crystal is related to the reflected-wave amplitude *via* the Fourier transform operation. Since only the reflected intensity is measured in practice there is therefore a phase problem in directly inverting such diffraction data to obtain the strain profile information, which is in some ways a microcosmic analog of the phase problem in conventional crystallography. More recently, Afanas'ev, Aleksandrov, Fanchenko, Chaplanov & Yakimov (1986) have claimed that measurement of reflectivity far into the tail of the dynamical peak can give information on the near-surface (static plus thermal) Debye-Waller factor down to a scale of the order of 10 Å. In particular, they showed theoretically that the asymptotic limit of the reflectivity curves gives the surface Debye-Waller factor (with the assumption that the surface is atomically flat).

Experiment and results

In the present study, triple-crystal measurements were carried out using both a conventional sealed X-ray tube and the Photon Factory synchrotron.

X-ray tube source

Fig. 3 shows the two-dimensional intensity distribution obtained for near-perfect symmetric Si(111) crystals as monochromator, sample and analyzer in a $(+n, -n, +n)$ configuration with Cu $K\alpha_1$ radiation from a conventional X-ray tube [fine (spot) focus; 40 kV, 20 mA]. Since the crystals were only about

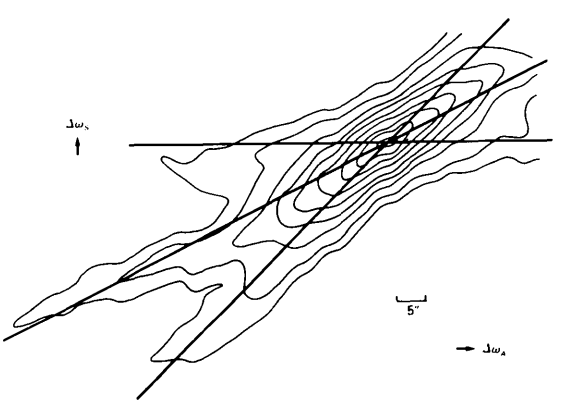

Fig. 3. Two-dimensional intensity distribution obtained with a conventional Cu X-ray tube for three near-perfect symmetric Si (111) crystals. The contour levels are 20 000, 15 000, 10 000, 5000, 2000, 1000, 500, 200 and 100 counts s^{-1}.

200 μm thick, great care was taken in mounting them to avoid any bending or strain. The Si(111) double-crystal rocking curve had a FWHM of approximately 11″, slightly larger than that of perfect Si. The FWHM of the dynamical tail from the sample, in $\Delta\omega_S$, is quite constant (for different values of $\Delta\omega_A$) at approximately 6″, indicating little or no surface roughness. Fig. 3 shows three distinct components which we associate with the dynamical tails of the three crystals (see Fig. 2). The range of intensities displayed in Fig. 3 is between two and three orders of magnitude.

Typical ω_S 'slice' scans, through the distribution in Fig. 3, show three distinct peaks. The first peak is at or close to $\Delta\omega_S = 0$ (tail of analyzer), the second at $\Delta\omega_S = \Delta\omega_A/2$ (tail of sample) and the third at $\Delta\omega_S = \Delta\omega_A$ (tail of monochromator).

A second symmetric Si(111) sample was studied with the experimental arrangement described above. This sample differed from the first in that it was approximately 6 mm thick and part of the surface had been subjected to ion implantation (Sb ions, 110 keV, 5×10^{15} cm^{-2}). The surface of this sample was polished and etched prior to ion implantation and annealed at 870 K for 30 min after ion implantation.

The Si(111) double-crystal rocking curve for the ion-implanted region of this second sample had a FWHM of approximately 11″. Fig. 4 contrasts the $\omega_S/2\omega_A$ slice scans through the central Si 111 peak (*i.e.* scans along the dynamical tail of the sample, where $\Delta\omega_S = \Delta\omega_A/2$) for the implanted and unimplanted regions of the sample. We see that, for the implanted region, the intensity on the low-angle side of the peak is larger and is smaller on the high-angle side, compared with that obtained for the unimplanted region (where the curve is symmetric about the peak position). This observation is consistent with the expected lattice-parameter variation in the near-surface region (and perpendicular to that surface) as a result of ion implantation.

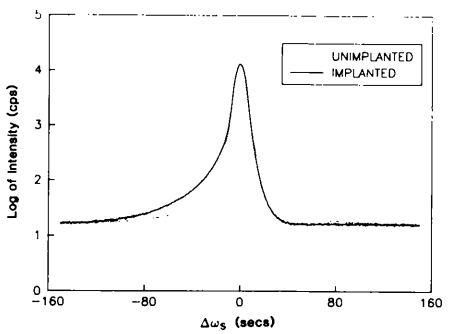

Fig. 4. $\omega_S/2\omega_A$ slice scans (X-ray tube source) through the central Si 111 peak for the implanted and unimplanted regions of the same sample. The two curves have not been scaled relative to each other.

Fig. 5 shows the location of various peaks, in ($\Delta\omega_S$, $\Delta\omega_A$) space, for several ω_S and ω_A slice scans, for the implanted region. The error bars are comparable with or smaller than the size of the points. Several additional small peaks were observed and are represented by triangles (with a distinction being made between those occurring in ω_S and ω_A slice scans). These small peaks seem to lie in the vicinity of either the $\Delta\omega_S$ axis or a line at approximately 135° to the positive $\Delta\omega_A$ axis and may be due to a combination of thermal diffuse scattering and lattice imperfections in the near-surface region. (The two peaks near the $\Delta\omega_S$ axis may also be indicative of a mosaic spread associated with the near-surface region of the sample.)

Synchrotron source

Triple-crystal diffraction experiments were carried out on a six-circle Huber diffractometer, located on beamline 4C at the Photon Factory [see Kashiwagura, Kashihara, Sakata, Harada, Wilkins & Stevenson (1987) for a description of the instrumental resolution function]. The experimental arrangement used is that depicted in Fig. 1. A wavelength of 1·387 Å was selected with the double-crystal Si(111) monochromator, with sagittal focusing (Matsushita, Ishikawa & Oyanagi, 1986). It proved possible to orient the analyzer and sample crystals very accurately, with respect to their ω rotations, by extrapolating peak positions in triple-crystal scans back to the line-crossing condition which determines the exact Bragg reflection setting for each crystal.

The first symmetric Si(111) sample we investigated with synchrotron radiation was one which had been

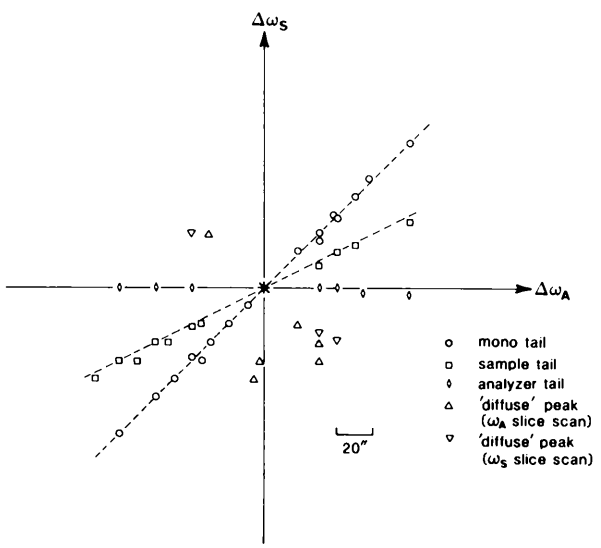

Fig. 5. Location of the various peaks, in ($\Delta\omega_S$, $\Delta\omega_A$) space, for the implanted region (X-ray tube source).

polished and etched but had some degree of surface roughness. This sample was unimplanted and approximately 1 mm thick. Fig. 6 shows ω_A slice scans for (*a*) $\Delta\omega_S = 0$, (*b*) $\Delta\omega_S = 0{\cdot}04°$, and a $2\theta_S$ slice scan for (*c*) $\Delta\omega_S = 0{\cdot}20°$. It is immediately obvious that carrying out triple-crystal diffraction studies with synchrotron radiation offers a very powerful method of characterizing the near-surface microstructure of crystalline samples of suitable quality. In this case the intensity distribution can be measured over eight orders of magnitude or more (*cf.* the present laboratory source results), enabling us to examine ($\Delta\omega_S$, $\Delta\omega_A$) space perhaps 50 times further away from the peak and thus more sensitively probing the near-surface region (*e.g.* Afanas'ev, Aleksandrov, Fanchenko, Chaplanov & Yakimov, 1986). It should be noted that the background level is extremely low, facilitating such detailed investigations.

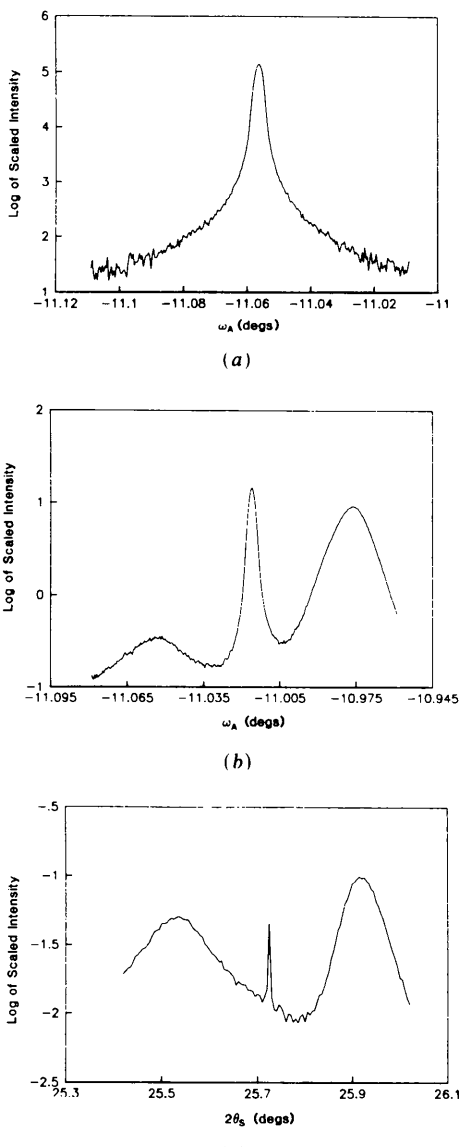

Fig. 6. ω_A slice scans at (*a*) $\Delta\omega_S = 0$, (*b*) $\Delta\omega_S = 0{\cdot}04°$, and a $2\theta_S$ slice scan at (*c*) $\Delta\omega_S = 0{\cdot}20°$ (synchrotron source).

Fig. 6 shows the expected peaks associated with the tails of the monochromator and sample. The FWHM of the monochromator peak is approximately 12″ and constant, whereas the FWHM of the sample peak increases systematically with increasing $\Delta\omega_S$, as shown in Fig. 7 (an analogous plot to Fig. 5), providing a quantitative measure of the degree of surface roughness [the value of σ as defined by Iida & Kohra (1979) being of order 1°]. Figs. 6 and 7 also show a relatively broad peak whose position in ($\Delta\omega_S$, $\Delta\omega_A$) space lies along a line at approximately 3° to the $\Delta\omega_S$ axis (*cf.* Fig. 5). The FWHM for this peak increases linearly with $\Delta\omega_S$, the data extrapolating to a FWHM of approximately 20″ at $\Delta\omega_S = 0$ and measuring approximately 0·3° at $\Delta\omega_S = 0{\cdot}4°$. This peak can be attributed, at least in part, to thermal diffuse scattering (the peak of which, for the isotropic case, is along a line at approximately 5° to the $\Delta\omega_S$ axis). There may also be effects due to sample mosaic spread and lattice imperfections in the near-surface region. The small marked region about the origin in Fig. 7 corresponds to the area of ($\Delta\omega_S$, $\Delta\omega_A$) space represented in Fig. 5 (and that which could practicably be measured with the laboratory source), further demonstrating the power of the triple-crystal technique with synchrotron radiation.

The second sample we investigated with synchrotron radiation was the ion-implanted crystal already described. Fig. 8 shows $2\theta_S$ slice scans from both the implanted and unimplanted regions for (*a*) $\Delta\omega_S = 0{\cdot}025$, (*b*) $\Delta\omega_S = 0{\cdot}05$ and (*c*) $\Delta\omega_S = 0{\cdot}25°$. In Fig. 8 we see the presence of a peak which is fixed at $2\theta_S \simeq 25{\cdot}52°$ (see previous comments) and is always

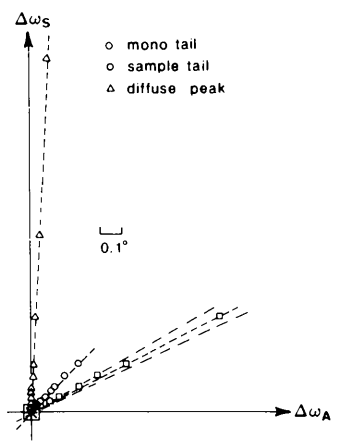

Fig. 7. Location of the various peaks, in ($\Delta\omega_S$, $\Delta\omega_A$) space (synchrotron source). The dot-dash lines represent the FWHM of the sample peaks, in $\Delta\omega_A$, and as such give a quantitative measure of the surface roughness.

somewhat wider and less intense for the implanted region. The FWHM for this peak increases more rapidly with $\Delta\omega_S$ for the implanted region. It should be noted that these 'diffuse' peaks were less intense for the previous Si sample, suggesting that imperfections and damage in the near-surface region have greater significance for the present Si sample. Fig. 8 also shows the narrow monochromator peaks and the sample peaks. The latter are less intense for the implanted region (*cf.* Fig. 4). The FWHMs for the sample peaks show a similar trend to those in Fig. 7.

Fig. 9 contrasts slice scans for which $\Delta\omega_S = \Delta 2\theta_S/2$ (*cf.* Fig. 4) for (*a*) the implanted and (*b*) the unimplanted regions. At the extremes of the plots the count rate was approximately 2 counts s^{-1}. Fig. 9(*a*) clearly shows oscillations in the intensity, from which one can estimate that the thickness of the strained region, resulting from the ion implantation, in the surface-normal direction is approximately 700 Å. This compares quite well with Monte Carlo calculations for the range of 110 keV Sb ions in Si, which give a maximum at approximately 600 Å, falling to about 10% at 1100 Å.

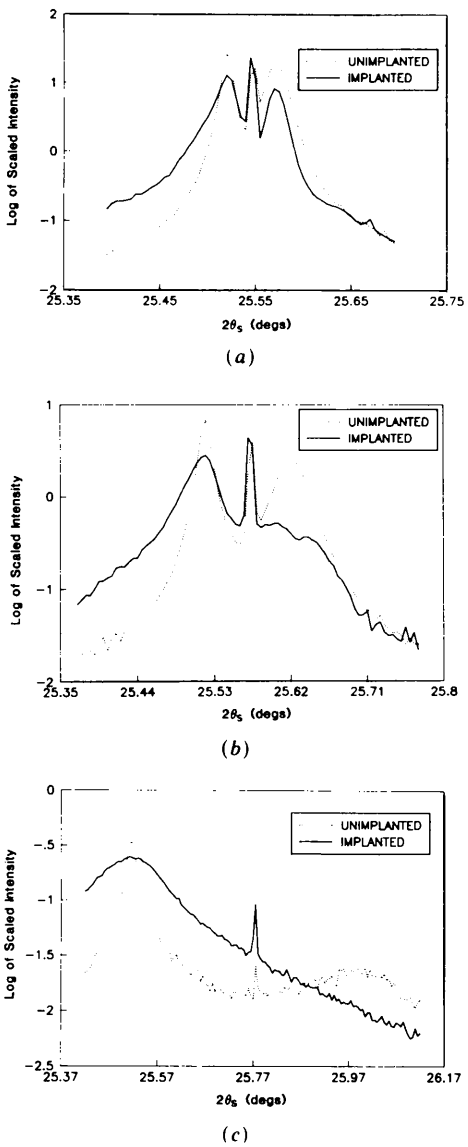

Fig. 8. $2\theta_S$ slice scans (synchrotron source) at (*a*) $\Delta\omega_S = 0{\cdot}025$, (*b*) $\Delta\omega_S = 0{\cdot}05$ and (*c*) $\Delta\omega_S = 0{\cdot}25°$ for the implanted and unimplanted regions of the same sample. The only scaling of data has been in accord with the monitor counts and reference scans.

Discussion

The results presented in this paper clearly demonstrate the power of the triple-crystal diffraction technique for the non-destructive characterization of near-perfect crystal samples on an atomic scale (*e.g.* Yakimov, Chaplanov, Afanas'ev, Aleksandrov, Imamov & Lomov, 1984). This is particularly true when the near-surface region is of interest (*e.g.* Iida & Kohra, 1979; Andrews & Cowley, 1985; Robinson, 1986; Kim, Gotoh, Takahashi, Ishikawa & Kikuta, 1986; Cowley & Ryan, 1987; Kashiwagura, Kashihara, Sakata, Harada, Wilkins & Stevenson, 1987), and the technique offers several advantages in comparison with double-crystal diffraction (*e.g.* Zaumseil, 1985). The use of synchrotron radiation facilitates the application of the triple-crystal technique, making possible the study of intensity variations over at least eight orders of magnitude.

In the present study the use of synchrotron radiation has been compared with the use of a conventional laboratory source. The presence of moderate surface roughness of the samples has been established, as have various effects of ion implantation.

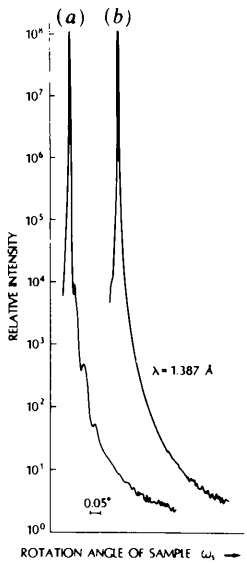

Fig. 9. Slice scans for which $\Delta\omega_S = \Delta 2\theta_S/2$ for (*a*) the implanted and (*b*) the unimplanted regions.

The authors wish to thank Professor J. Chikawa and the Photon Factory for providing the opportunity to carry out this work. The authors are most grateful to Professors H. Iwasaki and T. Matsushita of the Photon Factory for their encouragement, Dr A. Pogany for arranging the ion implantation of the Si sample, Dr S. Prawer for the Monte Carlo calculation and Dr S. Sasaki for supplying the Si analyzer crystal used at the Photon Factory. Two of the authors (AWS, SWW) gratefully acknowledge financial support from the Australian Department of Science under the Japan/Australia Bilateral Exchange Program.

References

AFANAS'EV, A. M., ALEKSANDROV, P. A., FANCHENKO, S. S., CHAPLANOV, V. A. & YAKIMOV, S. S. (1986). *Acta Cryst.* A**42**, 116-122.

AFANAS'EV, A. M., KOVAL'CHUK, M. V., KOVEV, E. K. & KOHN, V. G. (1977). *Phys. Status Solidi A*, **42**, 415-422.

ANDREWS, S. R. & COWLEY, R. A. (1985). *J. Phys. C*, **18**, 6427-6439.

COWLEY, R. A. & RYAN, T. W. (1987). *J. Phys D*, **20**, 61-68.

EISENBERGER, P., ALEXANDROPOULOS, N. G. & PLATZMAN, P. M. (1972). *Phys. Rev. Lett.* **28**, 1519-1522.

IIDA, A. & KOHRA, K. (1979). *Phys. Status Solidi A*, **51**, 533-541.

KASHIWAGURA, N., KASHIHARA, Y., SAKATA, M., HARADA, J., WILKINS, S. W. & STEVENSON, A. W. (1987). *Jpn. J. Appl. Phys.* **26**, L2026-L2029.

KIM, H., GOTOH, S. J., TAKAHASHI, T., ISHIKAWA, T. & KIKUTA, S. (1986). *Nucl. Instrum. Methods*, A**246**, 810-813.

MATSUSHITA, T., ISHIKAWA, T. & OYANAGI, H. (1986). *Nucl. Instrum. Methods*, A**246**, 377-379.

ROBINSON, I. K. (1986). *Phys. Rev. B*, **33**, 3830-3836.

WILKINS, S. W., CHADDERTON, L. T. & SMITH, T. F. (1983). *Acta Cryst.* A**39**, 792-800.

YAKIMOV, S. S., CHAPLANOV, V. A., AFANAS'EV, A. M., ALEKSANDROV, P. A., IMAMOV, R. M. & LOMOV, L. A. (1984). *JETP Lett.* **39**, 1-3.

ZAUMSEIL, P. (1985). *Phys. Status Solidi A*, **91**, K31-K33.

Acta Cryst. (1988). A**44**, 833-837

Reflection and Refraction of Fast Electrons at Solid/Solid Interfaces

BY J. TAFTØ

Research Centre, Norsk Hydro a.s, 3901 *Porsgrunn, Norway*

AND J. GJØNNES

Department of Physics, University of Oslo, Blindern, Oslo, Norway

(*Received* 15 *December* 1987; *accepted* 18 *April* 1988)

Abstract

The combined effects of refraction and reflection of fast electrons entering a thin specimen nearly parallel to an interface may be used to obtain quantitative information about the difference in the mean inner Coulomb potential (U_0) between the two adjoining phases. When no strong Bragg reflections are excited the electrons are deflected towards the phase with the largest $|U_0|$. By tilting the crystal so that strong Bragg reflections are excited some of the Bloch waves may be deflected in the opposite direction. The effect is demonstrated by simple two-beam calculations and observations for the Al/SiC interface.

Introduction

Whereas a variety of experimental techniques are available for the study of solid/vacuum interfaces, only a few methods are capable of providing information about buried interfaces. The most powerful technique for studying the structure of solid/solid interfaces may be TEM (transmission electron microscopy and diffraction). High-resolution imaging interpreted on the basis of the multi-slice formulation of Cowley & Moodie (1957) allows study of interface structures on an atomic scale (Ourmazd, Taylor, Rentschler & Bevk, 1987; Krakow, Wetzel & Smith, 1986). Several analytical techniques combined with a fine electron probe can be used to obtain profiles of composition on a nanometre scale. With electron energy-loss spectroscopy in particular, signals may be obtained from areas as small as 10 Å, including information about electronic structure as well (Batson, Kavangh, Wodall & Mayer, 1986).

In this paper we deal with a different TEM technique for extracting information about interfaces. The principle has been outlined briefly in a previous paper (Taftø, Jones & Heald, 1986). The deflection of the electron beam by the interface between two solids A and B due to the difference $\Delta U_0 = U_{0,A} - U_{0,B}$ between their mean inner potentials is used to form an image of the interface. This combined refraction/reflection effect may also be used to obtain electron energy loss spectra from the interfacial region.

The aim of the present paper is to present a further discussion of this technique, in particular the effect of Bragg reflection in one or both of the crystals and

0108-7673/88/060833-05$03.00